AUTHOR(S):

Sawamura, Yasuo; Inagami, Keita; Nishihara, Tomohiko; Kosaka, Takashi; Hattori, Masahiro; Kimura, Makoto

京都大学学術情報リポジトリ
KURENAI 紅
Kyoto University Research Information Repository

Technical Paper

Seismic performance of group pile foundation with ground improvement during liquefaction

Yasuo Sawamura [a,*], Keita Inagami [b], Tomohiko Nishihara [c], Takashi Kosaka [c]
Masahiro Hattori [d], Makoto Kimura [e]

[a] *Department of Urban Management, Kyoto University, Kyoto, Japan*
[b] *Technical Division, Technical Support Unit Facility Group, INPEX Corporation, Tokyo, Japan*
[c] *Construction Management Headquarters, Hanshin Expressway Company Limited, Osaka, Japan*
[d] *Division of Investigation Research, Hanshin Expressway Research Institute for Advanced Technology, Osaka, Japan*
[e] *Department of Civil and Earth Resources Engineering, Kyoto University, Kyoto, Japan*

Abstract

A pile foundation with ground improvement under the footing is a composite foundation with the objectives of enhancing the seismic performance and rationalizing the substructure by combining the pile foundation with ground improvement. Although the effectiveness of this method has been confirmed in previous studies for application to soft grounds, the applicability of this method to liquefiable grounds has yet to be fully investigated. In this study, therefore, centrifuge model tests and finite element analyses were conducted to clarify the effectiveness of this method and to ascertain the improvement in strength (stiffness) when the method is applied to a liquefiable ground. Firstly, in order to investigate the effect of an improved ground on the behavior of the pile foundation during liquefaction, dynamic centrifuge model tests were conducted for three cases with different strengths of the improved ground. Then, three-dimensional soil–water coupled finite element analyses of the centrifuge model experiments were performed to validate the applicability of the analytical method. After that, parametric studies, in which the strength of the improved ground and the input ground motion were changed, were conducted using the same analytical model. The results confirmed that the horizontal displacement of the pile heads was reduced by the improved ground even in the liquefiable ground, and that the effect of this reduction was more remarkable in cases of high stiffness of the improved ground. Furthermore, it was possible to reduce the bending moments at the pile heads by applying the ground improvement. However, since the bending moment at the boundary between the improved ground and the natural ground became the local maximum, there was an optimum stiffness of the ground improvement at which the maximum bending moment of the piles was reduced. This is because improving the ground around the pile heads has the same effect as extending the footing. It was thus concluded that the behavior of the pile foundation is similar to that of a composite foundation comprised of a caisson and group piles.
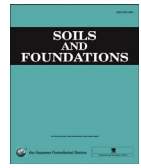© 2021 Production and hosting by Elsevier B.V. on behalf of The Japanese Geotechnical Society. This is an open access article under the CC BY-NC-ND license (http://creativecommons.org/licenses/by-nc-nd/4.0/).

Keywords: Pile foundation; Ground improvement; Liquefaction; Centrifuge model test; FEM

1. Introduction

In the design of pile foundations constructed on soft grounds or liquefiable grounds, the allowable horizontal displacement and stress intensity sometimes cannot be attained even when the allowable bearing capacity has been sufficiently secured. In such cases, countermeasures, like
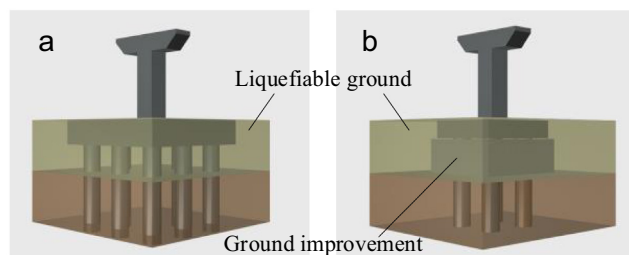

Fig. 1. Concept of pile foundation with ground improvement: (a) Traditional 3 × 3 group pile foundation and (b) 2 × 2 group pile foundation with ground improvement.

useing large piles or increasing the number of piles, will be taken. However, these countermeasures may lead to the enlargement of both the footing and the substructure. This will then result in problems, such as increases in the construction cost and construction period, and the need to expand the construction site. Especially in urban areas, where there are severe site restrictions due to site boundaries and existing structures, the enlargement of substructures is a major issue.

As a solution to the above problems, a method has been developed to rationalize substructures by performing ground improvement on the surrounding ground below the footing, as shown in Fig. 1. Improving the ground around the pile heads in the foundation enables an increase in the horizontal resistance of the pile-soil system, therefore reducing the pile diameter, the number of piles, and the footing size. Maeda et al. (2006, 2007) proposed two types of ground-improvement patterns depending on the depth of the bearing layer: improving the entire subsurface soft layer, and improving only the vicinity of the surface ground. They examined the horizontal bearing capacity of a composite pile foundation by horizontal loading tests at the site and conducted a numerical analysis. As a result, they reported that the horizontal resistance of the piles in both ground-improvement patterns was increased by improving the ground around the pile heads. Rollins et al. (2010) performed several full-scale lateral loading tests on a nine-pile pile group where ground-improvement techniques had been employed to increase the lateral resistance of the pile foundation. They reported that the increased lateral resistance of the pile group with the ground improvement could be explained by a simple model which accounts for the passive resistance behind the soil-mixed wall and the adhesive shear resistance along the sides and the base of the wall as the pile cap pushes the soil-mixed wall laterally. Tomisawa and Miura (2007) applied this method to a peat ground that was extremely soft and was not expected to have sufficient horizontal resistance with the construction of only the pile foundation. Furthermore, Tomisawa et al. (2008) performed a numerical analysis to evaluate the seismic performance of a composite pile foundation during an earthquake, and reported that the horizontal resistance of the piles was improved not only in terms of its static condition, but also in terms of its dynamic condition. In addition to the application of this method to new constructions, construction methods with ground improvement for the purpose of improving the seismic resistance of existing structures are also being studied. Bao et al. (2012) and Kheradi et al. (2019) conducted shaking table tests and a simulation to investigate the effect of the seismic enhancement of a group pile foundation with a partial ground-improvement method in dry sand and saturated sand, respectively. Tomisawa and Kimura (2017) conducted large shaking table tests using dry sand and saturated sand to evaluate the effect of liquefaction. As a result, it was reported that when the surrounding ground liquefies, the displacement of the pile heads can be suppressed by improving the ground at the pile heads. As described above, although the applicability of the composite foundation to soft grounds has been confirmed, its applicability to liquefiable grounds has only been examined under specific conditions and has not been sufficiently clarified.

The structural failure of piles passing through liquefiable soils has been observed in recent strong earthquakes. For example, Hamada and O'Rourke (1992) and Finn and Fujita (2002) analyzed the damage modes of pile foundations in liquefiable soils due to major earthquakes, such as the 1964 Niigata earthquake and the 1995 Hyogoken Nanbu earthquake. Bhattacharya et al. (2004, 2005) analyzed 15 reported cases of pile foundation performance during earthquake-induced liquefaction. They reported that, among the four patterns of failure (bending failure, bucking failure, shear failure, and settlement failure), the buckling failure of piles is observed when the thickness of the liquefiable layer is larger than the pile diameter. Pile foundations constructed in liquefiable grounds are prone to damage because the liquefaction reduces the horizontal resistance of the piles from the surrounding ground (e.g., Wilson et al., 2000; Rollins et al., 2005). Abdoun et al. (2003) conducted centrifuge model tests to analyze the seismic behavior of a pile foundation subjected to earthquake-induced liquefaction and lateral spreading. Phanikanth et al. (2013) analyzed the behavior of the soil–pile interaction in terms of inertial loads and kinematic interactions. In these studies, it was found that the depth of the liquefied layer has a significant influence on the pile-bending response, and that the peak bending moment will occur at the interface of the liquefied and non-liquefied layers.

The superiority of pile foundations with ground improvement has been confirmed for non-liquefied grounds, but in the event that the ground around the pile heads liquefies, the pile foundation will become a top-heavy structure, and the response of both the piles and the superstructure may be amplified. Furthermore, in addition to the influence of the boundary between the liquefied and the non-liquefied layers, there is also a boundary created by the ground improvement, so it is believed that the distribution of cross-sectional forces generated in the piles becomes more complicated.

In this study, therefore, centrifuge model tests and finite element analyses were conducted to understand the effect of improving the liquefiable ground around the pile heads on the behavior of the pile foundation during earthquakes. As a fundamental study on a composite pile foundation with ground improvement, the strength (stiffness) of the improved ground is a parameter that was changed while maintaining the same number of piles. Among the failure modes for piles in liquefied grounds, focus is placed on the bending failure mode of the piles because the liquefiable layer targeted in this study is thin compared with the pile diameter.

2. Centrifuge model tests

2.1. Experimental conditions

Dynamic centrifuge tests were conducted using the geotechnical beam centrifuge, with a radius of 2.5 m, located at the Disaster Prevention Research Institute (DPRI) at Kyoto University. The maximum centrifugal accelerations were 200g for the static tests and 50g for the dynamic tests. Dynamic loading was applied unidirectionally to the model through the shaking table by a servo-hydraulic actuator. The shaking direction was tangential to the arm rotation. The input motion of the shaking table was operated by a displacement control system. Therefore, calibration tests were performed prior to the model tests using the accelerometer installed on the shaking table to produce an input motion with the desired amplitude and frequency.

Fig. 2 presents a cross-sectional view of the experimental model. The experimental object was a 2 × 2 group pile foundation constructed on a ground consisting of a liquefiable layer 3 m from the surface and a non-liquefiable layer 10 m below the liquefiable layer. A rigid soil container, with a width of 450 mm, a height of 300 mm, and a depth of 150 mm, was used for the experiment. Because the pile model was placed at the center of the container and there was large space between the walls and the model, it is likely that the effect of the use of the rigid container was limited. There were three test cases, focusing on the presence or absence of an improved ground around the pile heads and the strength of the improved ground. All tests were performed at a centrifugal acceleration of 50g.

The response accelerations of the superstructure, pile heads, and ground were measured by pendulum-type accelerometers (A6H-50, SKS Co., Ltd.). In addition, five pore water pressure transducers (P306-A, SSK Co., Ltd.) were placed at five different depths in the model. Unlike the accelerometers, these sensors were attached to the back side of the soil container by water resistant double-stick tape so that their positions would not move during the experiment. The earth pressure acting on the improved ground was measured by earth pressure gauges (PDA-500KPB, Tokyo Measuring Instruments Laboratory Co., Ltd.). Laser displacement sensors (IL-100, KEYENCE
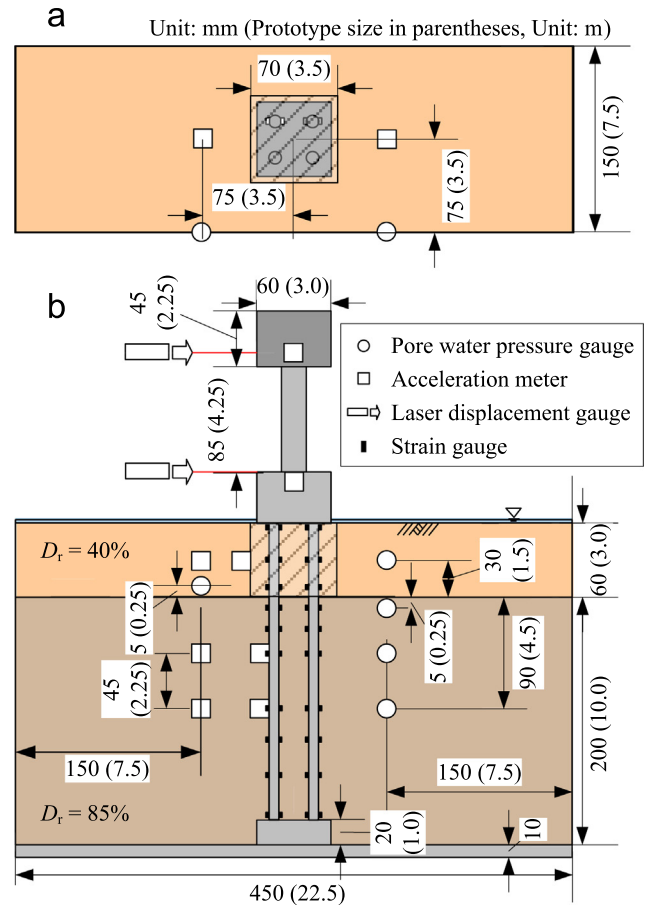

Fig. 2. Diagrammatic illustration of experimental setup in case of improved ground: (a) Top view and (b) Side view.

Corporation) were used to measure the horizontal displacement of the superstructure and the footing. The strain generated in the piles was measured by strain gauges (FLA-03-23-3LHT, Tokyo Measuring Instruments Laboratory Co., Ltd.). The strain gauges were attached to a front pile and a back pile in the direction of the vibration. A waterproof coating was applied to the piles to which the strain gauges were attached to protect the measurement area from water saturation and the improved ground.

Toyoura sand was used for both the liquefiable and the non-liquefiable layers. Table 1 shows the material properties of Toyoura sand. Fig. 3 show the photo taken when the non-liquefiable layer was prepared. The sand was prepared to achieve relative densities of 40% and 85% for the liquefiable and the non-liquefiable layers, respectively. The non-liquefied ground was made by tamping with a metal rod and a wooden plate until the model ground reached the predetermined height. The liquefiable layer was deposited by gently pulling up a funnel from the state at which the tip of the funnel was in contact with the ground surface and then moving it horizontally at a constant speed.

To satisfy the scaling law in the centrifugal field, a methylcellulose solution (Metolose (SM100), produced by

Table 1
Material properties of Toyoura sand.

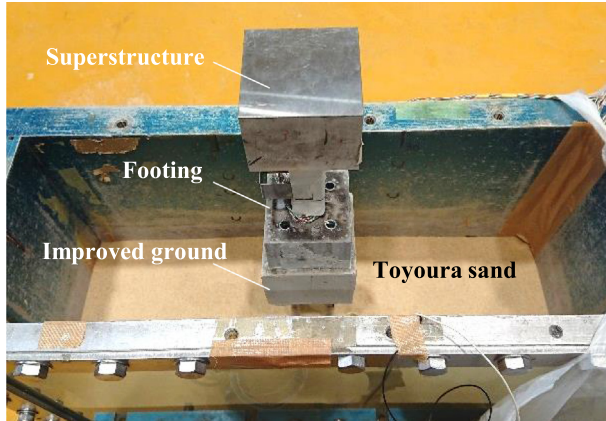|	
Specific gravity G_s	2.64
Average diameter D_{50} [mm]	0.20
Internal friction angle ϕ[deg]	38.9
Cohesion c [kPa]	0
Maximum void ratio e_{max}	0.975
Minimum void ratio e_{min}	0.585
Dry unit weight ($D_r = 40\%$) γ_d [kN/m³]	14.24
Dry unit weight ($D_r = 85\%$) γ_d [kN/m³]	15.76

Fig. 3. Preparation of experimental model.

Shin-etsu Chemical Co., Ltd. and adjusted to have a viscosity 50 times that of water, was employed. Metolose does not change the density or surface tension of a viscous fluid up to 100 mPa·s (Stewart et al., 1998; Dewoolkar et al., 1999). The viscosity of a Metolose solution depends strongly on the temperature of the fluid. The fluid temperatures of the ground surface before the tests in this study were 26.5 °C, 15.5 °C, and 17.5 °C for Cases-1, −2, and −3, respectively. Based on prior examination, the viscosities were estimated to be 57.5 cSt, 48.0 cSt, and 47.0 cSt, respectively. Although the viscosities in Cases-2 and 3 were close to 50 cSt, that in Case-1 was larger than the desired value. Therefore, in Case-1, it is thought that the increase in excess pore water pressure due to the ground motion and the subsequent dissipation may have proceeded at slower rates than in the other two cases.

The model ground was saturated in a deaeration container. Firstly, a vacuum pressure of about −0.1 MPa was applied, and then the air in the voids was replaced with carbon dioxide. After the vacuum pressure was reapplied, the saturated methylcellulose solution was dropped onto the ground surface from a tube installed inside the deaeration container. The ground was saturated for about 12 h. The degree of saturation was measured by the vacuum-chamber method (Okamura and Inoue, 2012). The degrees of saturation in all three cases were higher than 99.9%.

Steel pipe piles, with a length of 12 m, a diameter of 0.4 m, and a thickness of 0.04 m in prototype scale, were

modeled. The model piles were made of aluminum alloy and had a Young's modulus of 6.83×10^7 kN/m². The section dimensions of the model piles (diameter: $D = 8$ mm and thickness: 0.8 mm in model scale), which determined the second moment of the area (I), were calculated such that the bending stiffness (EI) of the pile in prototype scale would be the same as that of the assumed research object. The length of the model piles was 30 mm in model scale, and both ends of the piles were fixed by aluminum blocks. The piles were adhesively fixed to the aluminum blocks using an epoxy adhesive (tensile strength of 10,000 kN/m² or higher). The pile spacing was set to $4.0D = 32$ mm, considering the workability for casting the improved soil and fixing the pile model to the soil container. The spacing between the piles and the footing edge was $1.75D = 14$ mm. The aluminum block at the pile tip was screwed to the base plate.

In order to analyze the pile foundation performance during earthquake-induced liquefaction, Bhattacharya et al. (2004, 2005) introduced two parameters, namely, r_{min} (minimum radius of gyration) and L_{eff} (effective buckling length of the pile), and their ratio (L_{eff}/r_{min}) as the slenderness ratio of the piles. They suggested that columns having slenderness ratios below 50 are expected to fail due to plastic squashing, whereas those with ratios above 50 are expected to fail due to buckling, both modes being modified by induced bending moments. In this experimental model, r_{min} and L_{eff} were 0.0768 and 1.5, respectively; and thus, the slenderness ratio of the piles was 19.5, which is below 50. Therefore, among the failure modes for piles in liquefied grounds, focus was placed on the bending failure mode of the piles.

In addition to the superstructure ($60 \times 60 \times 45$ mm in model scale), made of a stainless steel block ($E = 1.97 \times 10^8$ kN/m²), the bridge pier ($20 \times 20 \times 100$ mm in model scale), made of an aluminum block ($E = 6.83 \times 10^7$ kN/m²), was also modeled to consider the center of gravity of the superstructure.

In order to investigate how the behavior of the piles differs depending on the strength of the ground improvement around the pile heads, and how this difference affects the behavior of the pile foundation during liquefaction, centrifuge model tests were conducted for three cases. In Case-1, the ground around the pile heads was not improved. In Cases-2 and −3, ground improvements with relatively low and high strengths were applied, respectively. The strength of the improved ground in Case-2 was determined with reference to an actual example (Shinohara et al., 2015) where the method was applied. The target strength of the improved ground was $q_u = 600$ kN/m², and the improved ground was made with a dry weight ratio of Kasaoka clay: early strength Portland cement: water of 8: 1: 5.61. The strength of the improved ground in this experiment was $q_u = 1100$ kN/m². On the other hand, in Case-3, the improved ground was made with a dry weight ratio of Kasaoka clay: silica sand No. 6: early strength Portland cement: water of 1:2:1:1.27, so that the strength

Table 2
Material properties of improved ground.

|	Case-2 (Low strength)	Case-3 (High strength)
Unconfined compressive strength q_u [kN/m^2]	1100	9030
Young's modulus E [kN/m^2]	8.82×10^5	7.53×10^6
Poisson's ratio v	0.20	0.21
Density ρ [g/cm^3]	1.57	1.90

Fig. 4. Input wave: (a) Time history of acceleration measured at shaking table in Case-1 and (b) Fourier spectrum of measured wave and Level 1 earthquake.

of the improved ground would be 10 times that of Case-2. The strength of the improved ground in Case-3 was $q_u = 9030$ kN/m^2. Table 2 shows the material properties of the improved ground for both Case-2 and Case-3. The size of the improved ground was 70×70 mm, which was also determined based on a real example (Shinohara et al., 2015).

In an actual construction, the pile foundation is constructed after the ground has been improved. However, it is difficult to reproduce this construction process in a model test. Therefore, in the present experiment, the improved ground was cast around the pile heads in advance. The improved ground was cured by sealing for 24 h and then cured in water for 7 days. These casting and curing processes were performed in a room with a constant temperature of 20 °C and humidity of 60%. In the preparation of the experimental models, as shown in Fig. 3, the pile foundation with the improved ground was firstly installed in the soil container, and then the ground was put in the container and tamped to achieve the specified density, as previously mentioned.

Regarding the input wave, the aim was to input a Level 1 earthquake (Japan Road Association, 2012a), which is used for the design of road bridges in Japan. Since the shaking table is operated by a displacement control system, the target acceleration was integrated twice, and the baseline-corrected displacement was input into the shaking table. Fig. 4 shows the time history of the acceleration and the Fourier spectrum observed on the shaking table in the experiment.

2.2. Experimental results

Fig. 5 shows the time histories of the excess pore water pressure ratios (EPWPRs) of the ground. The excess pore water pressure was calculated by subtracting the initial pore water pressure (hydrostatic pressure), at the centrifugal acceleration of $50g$, from the measured value of the pore water pressure gauge. The initial effective stress was calculated from the submerged unit weight assuming that the model ground was made with the predetermined relative densities.

At GL -1.5 m, which is at the center of the liquefiable layer, the EPWPRs in all three cases were 1.0 or close to 1.0 at around 5 s, which means that the ground was
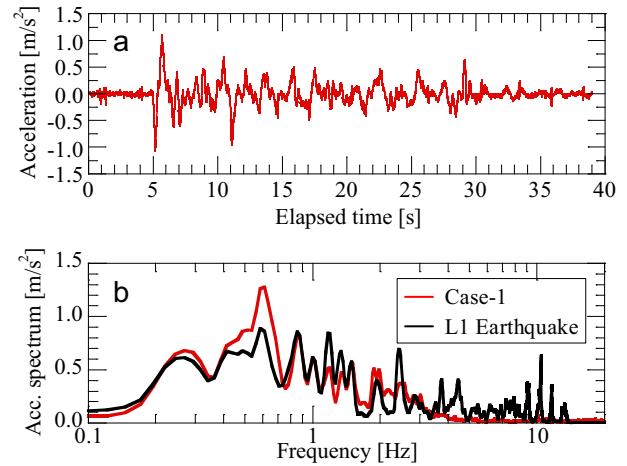
liquefied. Even at the lower end of the liquefiable layer (GL -2.75 m), the EPWPRs were about 0.8, indicating that the strength of the ground decreased with the decrease in effective stress. Tamura et al. (1999) reported that the stiffness of the ground during liquefaction decreases sharply when the EPWPR becomes 0.4 or more.

On the other hand, in the non-liquefiable layer, although large EPWPRs of about 0.8 were measured near the boundary with the liquefiable layer (GL-3.25 m), they were about 0.3 at the center of the non-liquefiable layer (GL -7.5 m). Therefore, it is thought that the non-liquefiable layer had a certain degree of strength during the excitation.

In this study, both the liquefiable and the non-liquefied layers were made of Toyoura sand, and the resistance to liquefaction was expressed only by the difference in relative density. Although relatively large EPWPRs were observed in the vicinity of the boundary between the two layers, even in the non-liquefiable layer, it is believed that the ground conditions and the input ground motion were reproduced as intended. However, the trends in the dissipation of the EPWPRs are different among the three cases. The difference in EPWPRs is thought to be due to the difference in viscosity of the Metolose solution, as mentioned above.

Figs. 6 and 7 show the time histories of the response acceleration at the pile heads and the Fourier spectrums, respectively. Fig. 6 shows the entire excitation range and an enlarged view of the period from 5 to 15 s. As large response acceleration and response displacement of the pile heads occurred during the period of 5 to 15 s, causing large bending moments of the pile, the results obtained during this period were given special attention in the subsequent data analyses. Regarding the presence or absence of the improved ground, the amplitudes of the response acceleration in Cases-2 and -3 with ground improvement are slightly suppressed compared to that in Case-1 without improvement. On the other hand, regarding the strength of the ground improvement, there was no clear difference
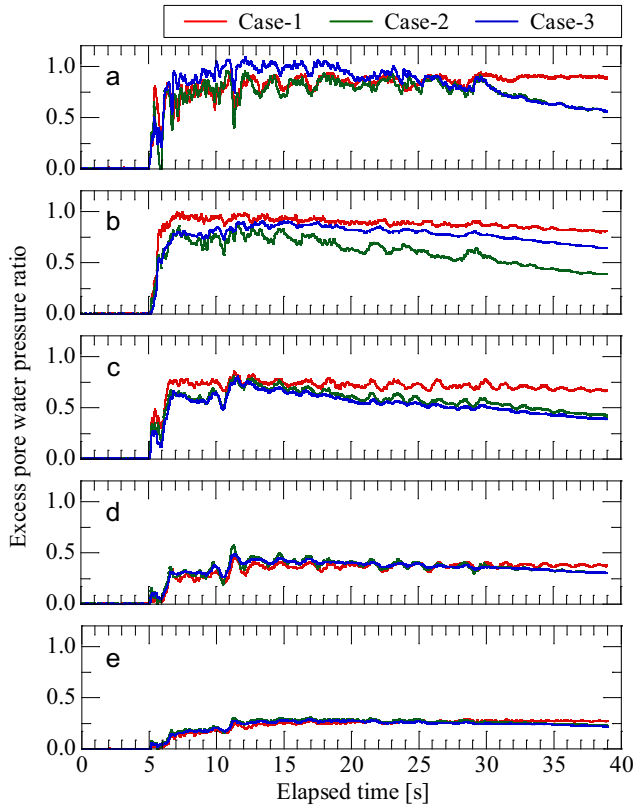
Fig. 5. Time histories of excess pore water pressure ratios of ground (centrifugal model tests): (a) GL −1.5 m, (b) GL −2.75 m, (c) GL −3.25 m, (d) GL −5.25 m, and (e) GL −7.5 m.

Fig. 7. Fourier spectrum of response acceleration at pile heads.

between Cases-2 and −3. From Fig. 7, it can be seen that the response spectrums near 0.6 Hz in Cases-2 and −3 are smaller than that in Case-1. However, there was almost no difference in terms of the presence or absence of improvement at other frequencies, and the response of the piles did not increase due to the ground improvement. In addition, no changes were observed in the response
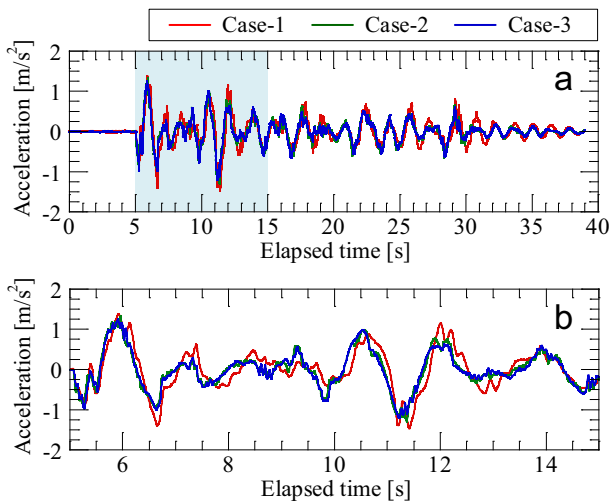
characteristics in the frequency domain due to the ground improvement.

Fig. 8 shows the time histories of the horizontal displacement of the pile heads. Similar to Fig. 6, Fig. 8 shows the entire excitation range and an enlarged view of the period from 5 to 15 s. The amplitudes of the displacement in Cases-2 and −3 are seen to have significantly decreased. Under the experimental conditions, the decreasing effect by the ground improvement was particularly remarkable at 6 to 14 s and after 25 s. In other words, it can be said that even after the ground has completely liquefied, the displacement of the pile heads can be reduced by restraining the pile heads by the improved ground. Focusing on the maximum displacement, it was 0.0574 m (11.475 s) in Case-1, 0.0380 m (11.395 s) in Case-2, and 0.0353 m (11.410 s) in Case-3. The maximum displacements of the pile heads for Cases-2 and −3 were 34% and 39% lower, respectively, than that for Case-1. By increasing the stiffness of the improved ground, the maximum displacement of the pile heads was strongly suppressed, which was qualitatively consistent with the results of previous studies on soft grounds through static tests (Rollins et al., 2010).

Fig. 9 shows the distribution of bending moments of the piles when the horizontal displacement of the pile heads reaches the local maximum or minimum. In this paper, the increment in bending moment from the time the cen-

Fig. 6. Time histories of response acceleration at pile heads: (a) Whole time and (b) 5 to 15 s.

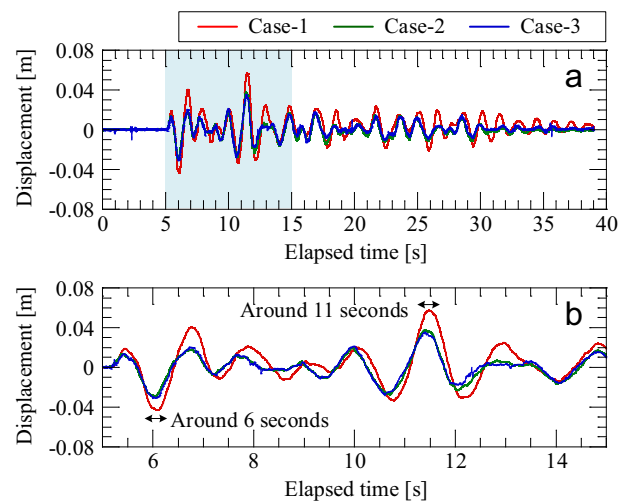Fig. 8. Time histories of horizontal displacement of pile heads: (a) Whole time and (b) 5 to 15 s.

京都大学
KYOTO UNIVERSITY

A Self-archived copy in
Kyoto University Research Information Repository
https://repository.kulib.kyoto-u.ac.jp

KURENAI 紅
Kyoto University Research Information Repository

trifugal acceleration reaches 50g is used. Due to measurement defects in the strain gauges, the bending moments at GL −8.75 m in Case-1 and at GL −0.25 m in Case-2 could not be calculated. As shown in Fig. 5, even in the non-liquefied layer, the stiffness of the ground decreased due to the increase in the EPWPR from 6 s to 15 s. In all cases, the bending moment distributions around 11 s have an inflection point near GL −4.25 to −5.25 m which is lower than that around 6 s. This is because the EPWPRs above this point were larger than 0.4, and the stiffness of the ground was significantly degraded. From Fig. 9, it can be seen that the bending moment at the pile heads is always reduced by the improved ground even if the degradation levels of the ground stiffness due to the liquefaction and the displacement of the pile head are different. Furthermore, in cases with the ground improvement, the bending moment reaches the local maximum at the boundary between the improved ground and the natural ground, and the maximum bending moment in cases with higher stiffness of the improved ground is larger. In this experiment, the distribution of bending moments in cases with ground improvement was shown so that the lower part of the improved ground performs as the pile heads, as if the footing were extended by the ground improvement. This behavior supports the theory (Maeda et al., 2006) that a caisson and a pile foundation can be treated as a composite structure when high-strength ground improvement is applied to a narrow area around the pile heads.

3. Reproduction analyses of centrifuge experiments

3.1. Analytical conditions

Three-dimensional soil–water coupled finite element analyses were performed to simulate the centrifuge model tests based on the infinitesimal deformation theory using the finite element analysis code DBLEAVES (Ye et al., 2007). Through the analyses, the applicability of the analytical method was validated. Then, parametric studies were conducted using the same analytical model in order to evaluate the effect of the improved ground on the behavior of the piles during liquefaction. In these parametric studies, the strength of the improved ground and the input ground motion were changed.

Fig. 10 shows the analytical mesh and boundary conditions used for the reproduction analyses. The mesh had 12,880 nodes and 8046 elements. The displacement at the bottom of the analytical domain was fixed in all directions to input seismic motions. The drainage conditions were set so that the ground surface was the drainage boundary and the other areas were non-drainage boundaries.

The mechanical properties of the ground were represented by the cyclic mobility model (Zhang et al., 2007). In addition to the concepts of superloading, related to the soil skeleton structure (Asaoka et al., 1998), and subloading, related to the density (Hashiguchi and Ueno, 1977), a new approach was introduced in this model to describe the stress-induced anisotropy.

Fig. 11 shows the subloading, normal, and surperloading yield surfaces in the p-q plane (Asaoka et al., 2002) as well as the changes in the subloading yielding surfaces
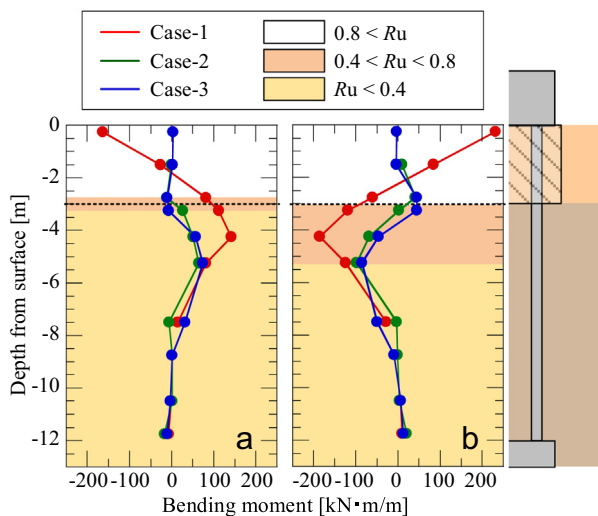

Fig. 9. Distribution of bending moments of pile when displacement at pile heads becomes local maximum or minimum value: (a) Around 6 s and (b) Around 11 s.
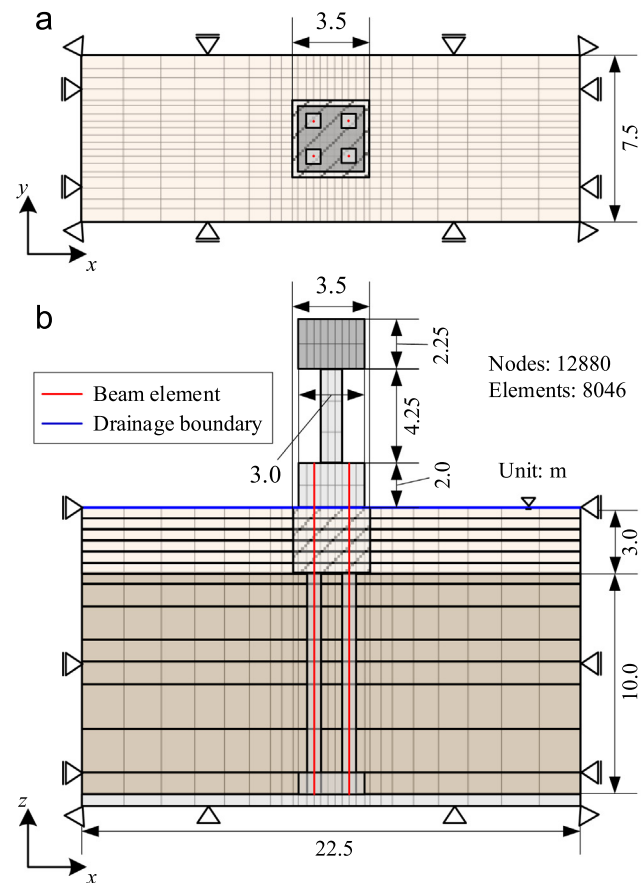

Fig. 10. Analytical mesh and boundary conditions: (a) Top view and (b) Side view.

at different anisotropy ζ (Zhang et al., 2007). The normal yield surface is given in the following form:

$$f = \ln\frac{p}{\tilde{p}_0} + \ln\frac{M^2 - \zeta^2 + \eta^{*2}}{M^2 - \zeta^2} + \ln R^* - \ln R - \frac{\varepsilon_V^p}{C_p} = 0 \qquad (1)$$

The variables involved in Eq. (1) are defined in the general stress state as

$$p = \frac{1}{3}\sigma_{ii} \qquad (2)$$

$$\eta^* = \sqrt{\frac{3}{2}\hat{\eta}_{ij}\hat{\eta}_{ij}}\hat{\eta}_{ij} = \eta_{ij} - \beta_{ij}\eta_{ij} = \frac{S_{ij}}{p} = \frac{\sigma_{ij} - p\cdot\delta_{ij}}{p} \qquad (3)$$

$$\eta = \sqrt{\frac{3}{2}\eta_{ij}\eta_{ij}}\zeta = \sqrt{\frac{3}{2}\beta_{ij}\beta_{ij}} \qquad (4)$$

$$C_p = \frac{\lambda - \kappa}{1 + e_0} \qquad (5)$$

where s_{ij} is the deviatoric stress tensor, β_{ij} is the anisotropic stress tensor, and σ_{ij} is the Cauchy effective stress tensor. λ and κ represent the compression and the swelling index, respectively.

The similarity ratio of the superloading yield surface to normal yield surface R^* and the similarity ratio of the superloading yield surface to subloading yield surface R are the same as those in the work by Asaoka et al. (2002), as follows,

$$R^* = \frac{\tilde{p}}{\bar{p}} = \frac{\tilde{q}}{\bar{q}}, 0 < R^* \leqslant 1 \text{ and } \frac{\tilde{q}}{\tilde{p}} = \frac{\bar{q}}{\bar{p}} \qquad (6)$$

$$R = \frac{p}{\tilde{p}} = \frac{q}{\tilde{q}}, 0 < R \leqslant 1 \text{ and } \frac{\tilde{q}}{\tilde{p}} = \frac{\bar{q}}{\bar{p}} = \frac{q}{p} \qquad (7)$$

where (p,q), $(\tilde{p},\tilde{q})$, and $(\bar{p},\bar{q})$ represent the present stress state, the corresponding normally consolidated stress state, and the structured stress state at the p-q effective stress space, respectively, which is only related to the conventional triaxial stress ($\sigma_{22} = \sigma_{33}$, q = σ_{11}-σ_{33}).

The consistency equation for the subloading yield surface can then be given as

$$df = \frac{\partial f}{\partial\sigma_{ij}}d\sigma_{ij} + \frac{\partial f}{\partial\beta_{ij}}d\beta_{ij} + \frac{1}{R^*}dR^* - \frac{1}{R}dR - \frac{1}{C_p}d\varepsilon_V^p = 0 \qquad (8)$$

where $d\beta_{ij}$, dR^*, and dR represent the rates of the degrees of anisotropic stress, structure, and overconsolidation, respectively.

In this model, particular attention was paid to the description of the sand subjected to cyclic loading under undrained conditions. In other words, for loose sand, liquefaction will occur without transition from the contractive state to the dilative state; for medium dense sand, cyclic mobility will occur; for dense sand, liquefaction will not occur. Among the eight parameters involved in the model, five parameters, M, N, λ, κ, and v, were the same as in the Cam-clay model, which can be determined by drained triaxial compression tests. The other three parameters (a, m, and b_r) had clear physical meanings and were determined by undrained triaxial cyclic loading tests and drained triaxial compression tests. Table 3 shows the material parameters of Toyoura sand determined in previous researches (Zhang et al., 2010, 2011). Figs. 12 and 13 show the results of simulations of drained triaxial compression tests and undrained cyclic loading tests for the liquefiable layer with a relative density of 40% and the non-liquefiable layer with a relative density of 85%. The confining pressure at the center of each layer was used for the initial confining pressures in the simulations.

In order to examine the fundamental behavior of pile foundations with ground improvement under the footing during liquefaction, the piles and superstructures were modeled with elastic bodies. Each pile was modeled by the hybrid element proposed by Zhang et al. (2000), which is composed of a beam element and solid elements, to take into consideration the volume of the piles. The stiffness of each pile is shared by the beam element and the neighboring solid elements in such a way that the bending stiffness
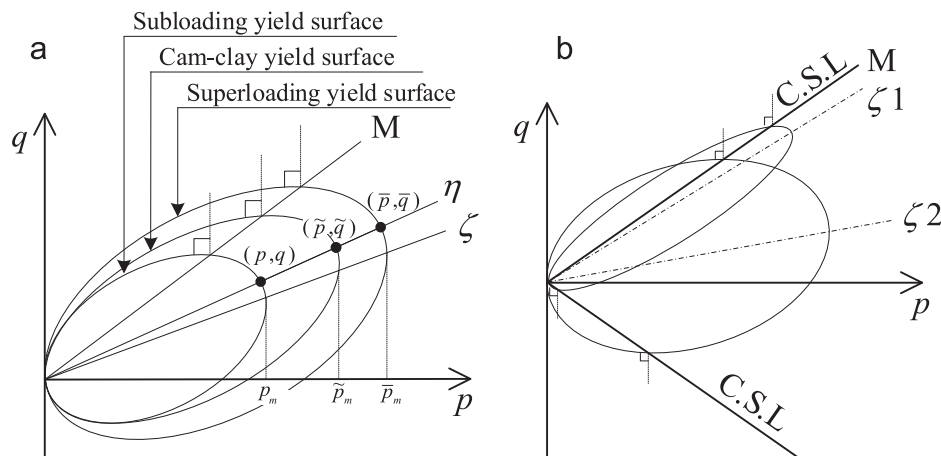

Fig. 11. Concepts of constitutive model used for Toyoura sand: (a) Subloading, normal and surperloading yield surfaces in p-q plane (after Asaoka et al., 2002) and (b) Changes in the subloading yielding surfaces at different anisotropy ζ (after Zhang et al., 2007).

Table 3
Material properties of Toyoura sand used for analysis.

	Toyoura sand
Critical state parameter M	1.30
Compression index λ	0.05
Swelling index κ	0.0064
Void ratio N (p' = 98 kPa on NCL)	0.87
Poisson's ratio v	0.30
Permeability k [m/s]	5.7×10^{-4}
Degradation parameter of overconsolidation state m	0.01
Degradation parameter of structure a	0.5
Evolution parameter of anisotropy b_r	1.5
Initial degree of structure R^*_0	0.80
Initial anisotropy $\varsigma 0$	0.0
Initial void ratio e_0	0.644 ($D_r = 85\%$), 0.819 ($D_r = 40\%$)

of pile EI is equal to the sum of the bending stiffness of the beam element and that of the solid elements. The best sharing ratio of bending stiffness between the beam element and the solid elements was found to be 9 to 1 (Zhang et al., 2000), which is also used in the calculation in this paper. However, in the footing, the improved ground and the aluminum block at the pile tip, where the pile is enclosed by highly stiff material other than soil, there is concern that the behavior will be adversely affected because elastic elements with low stiffness exist between the beam element and the surrounding stiffer materials. Therefore, a hybrid element model was not used for the footing, the improved ground or the aluminum block in this analysis.

Since the behavior of the improved ground changes greatly depending on the strength and stiffness, it should be able to be modeled by an elastoplastic constitutive model. Therefore, the improved ground was represented by the Modified Drucker-Prager model (Zhang et al., 2000). Zhang et al. (2000) added a simple modification to the original Drucker-Prager model in such a way that, when the stress state is on the failure line and the increment in stress is judged as loading, an adjustment has to be made to maintain the stress state on the failure line. The simple method adopted here is to let Young's modulus be a very small value and to follow the flow rule for the plastic strain. This modification allows the shear strength of the soil to remain almost constant on the failure line. By assuming

$c = q_u/2$ and $\phi = 0$, the material parameters of the improved ground can be easily identified through uniaxial compression tests because only four parameters need to be determined.

The input ground motion used in the analyses is the time history of the acceleration measured at the shaking table during the experiment, as shown in Fig. 4. The viscous damping and the direct integration method of Newmark-β ($\beta = 121/400$, $\gamma = 3/5$) was used, and the time interval of the calculation was 0.002 s, which is 1/5 of the measurement interval in the centrifugal model tests.

3.2. Analytical results

Fig. 14 shows the time histories of EPWPRs at the ground in Cases-1 and −2. At GL −1.5 m, the process for the increase in EPWPRs is reproduced well from the beginning of the excitation. At GL −2.75 m, the EPWPRs in the experiments rose sharply from the beginning of the excitation, reached a peak value around 7 s, and then began to gradually dissipate. On the other hand, in the analyses, the EPWPRs reached the peak value with a delay (around 13 s), and there was no tendency for them to dissipate. Both the delay of the increase in EPWPRs and the lack of any tendency for their dissipation in the reproduction analysis have also been reported in a previous research (Kheradi et al., 2019), which simulated 1G shaking table tests for piles constructed in a liquefiable layer using the same model as in this study. The phenomenon is thought to be due to the difference in the permeability of the liquefied grounds between the experiment and the simulation. Arulanandan and Sybico (1992) reported that the permeability of the liquefied ground increases from the value at the initial state due to the change in the soil structure. In addition, in order to reproduce the experiment by the simulation, Yoshida and Finn (2000) showed that it is necessary to increase the permeability of the ground immediately after liquefaction and return it to the initial value with the dissolution of excess pore water pressure. In this study, because the permeability of the liquefied ground did not change even after liquefaction, it is believed that the processes for the increase and dissipation of the excess pore water pressure could not be perfectly reproduced.
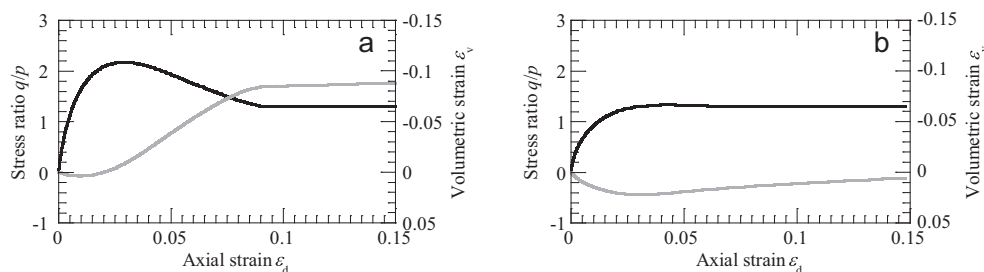

Fig. 12. Simulation of triaxial compression tests (CD) for different relative densities: (a) $D_r = 85\%$ with initial confining pressure of 70 kPa and (b) $D_r = 40\%$ with initial confining pressure of 13 kPa.
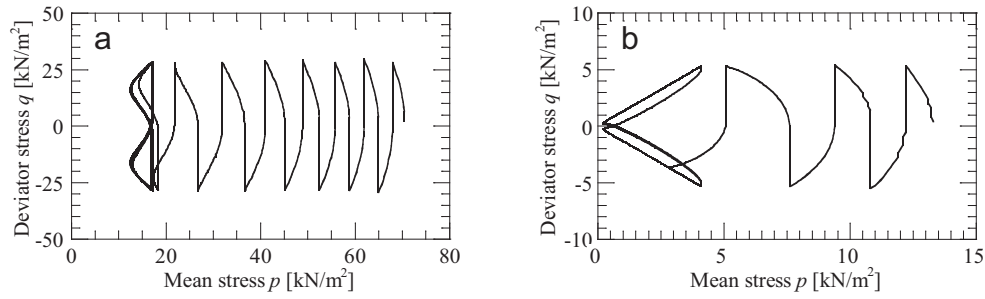
Fig. 13. Simulation of CU cyclic loading tests for different relative densities under stress ratio of 0.2: (a) $D_r = 85\%$ with initial confining pressure of 70 kPa and (b) $D_r = 40\%$ with initial confining pressure of 13 kPa.

At GL -5.25 m, the process for the increase in the EPWPRs is reproduced well, but that for the dissipation of the EPWPRs is delayed with respect to the experimental values, as with the shallower positions. Compared to the results at GL-5.25 m, the delay in the dissipation of the EPWPRs is small at GL-7.5, and the experiments are reproduced well throughout the excitation. From the results of these analyses, the EPWPRs of the ground above GL-5.25 m are seen to be smaller than the experimental values up to 15 s; and thus, the analyses may yield higher levels of stiffness of the ground than the experiment. On the other hand, after 15 s, the analytical values are larger than the experimental ones for all layers, and the stiffness of the ground is evaluated to be smaller.

Fig. 15 shows the time histories of the response acceleration in the ground in Case-2. Since the results of the experiments and the analyses showed almost the same acceleration of the ground, regardless of the presence or absence of an improved ground and strength of the improved ground, only the results of Case-2 are shown in the figure. At GL-1.5 m, which is in the liquefied layer, the analysis reproduces the experiment well on the whole, but small increases and decreases due to the high frequency components are not reproduced. However, in the non-liquefied layer, the analysis accurately reproduces the experimental results because no waves of the high-frequency components were observed in the experiment.

Fig. 16 shows the time histories of the response acceleration at the pile heads. Regarding the increases and decreases in amplitude, the analyses almost reproduced the experiments. Although the phases of the response acceleration have generally been reproduced, the analytical values tend to peak slightly earlier than the experimental values, and this tendency is more pronounced in Cases-2 and -3 which include the ground improvement. As mentioned above, one of the reasons for this is that, in this
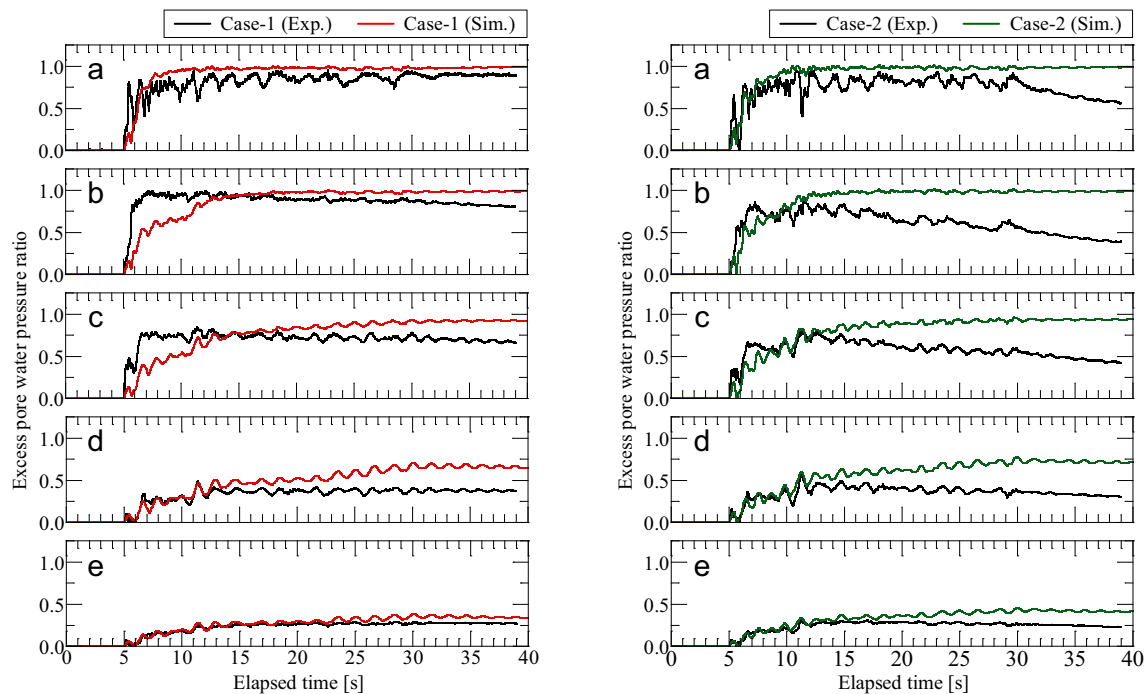

Fig. 14. Time histories of excess pore water pressure ratios of ground in Cases-1 and -2 (centrifugal model tests and simulations): (a) GL -1.5 m, (b) GL -2.75 m, (c) GL -3.25 m, (d) GL -5.25 m, and (e) GL -7.5 m.
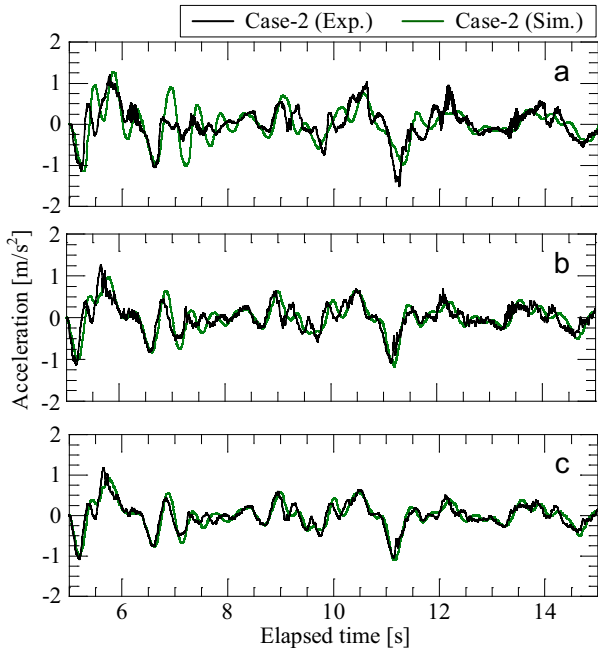
Fig. 15. Time histories of response acceleration of ground in Case-2 (centrifugal model tests and simulation): (a) GL −1.5 m, (b) GL −5.25 m, and (c) GL −7.5 m.

analyses, the increase in the EPWPRs tends to be delayed from the beginning of excitation to around 15 s, and the ground stiffness is slightly overestimated. Therefore, the propagation of the acceleration might have increased

because the stiffness of the ground determined in the analyses was more overestimated than that in the experiments.

Fig. 17 shows the time histories of the response displacement of the pile heads. Similar to the acceleration at the pile heads, although the displacements are reproduced as a whole, the difference in phases between the analyses and the experiments are large and the amplitudes in the analyses are also large compared to the experiments, especially in Cases-2 and −3.

Fig. 18 shows the distribution of bending moments of the piles when the time history of the response displacement of the pile heads becomes the local maximum or minimum value. The analyses reproduce the experiments well at both times, but the shapes of the distribution were closer to experimental one at around 11.4 s. This is because the distribution of bending moments depends on the reproduction of the EPWPRs.

Fig. 19 shows a comparison of the experimental and numerical results for the maximum pile head displacements and the maximum bending moments. The maximum pile head displacement and the maximum bending moment both occurred around 11 s. From the figure, it is confirmed that the difference due to the presence or absence of ground improvement and the improvement strength has been sufficiently evaluated, although the pile head displacements and the bending moments of the analytical results are slightly larger and smaller, respectively, than the experimental results.
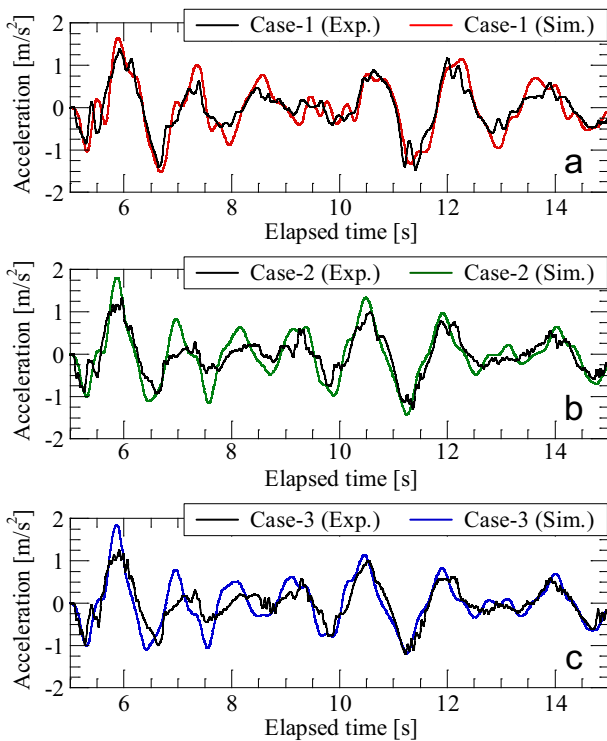

Fig. 16. Time histories of response acceleration at pile heads (centrifugal model tests and simulations): (a) Case-1, (b) Case-2, and (c) Case-3.
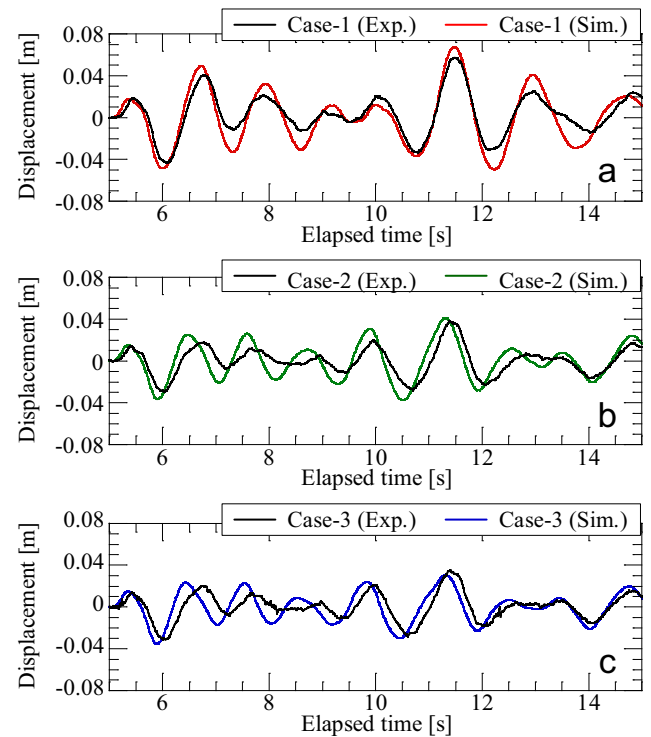

Fig. 17. Time histories of response displacement of pile heads (centrifugal model tests and simulations): (a) Case-1, (b) Case-2, and (c) Case-3.
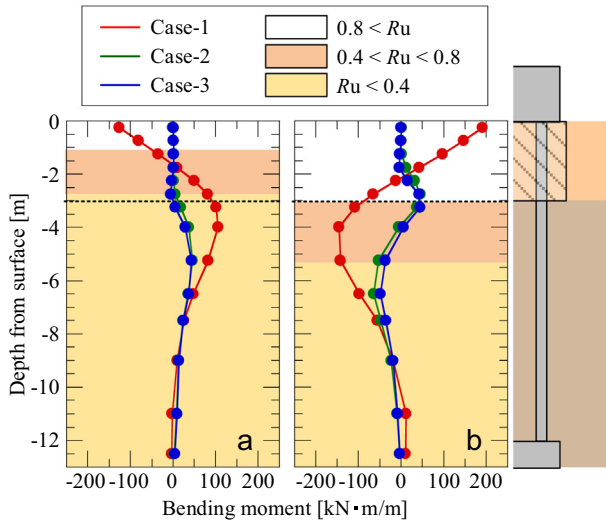
Fig. 18. Distribution of bending moments of pile when time history of response displacement at pile heads becomes local maximum or minimum value (simulations): (a) Around 6 s and (b) Around 11 s.

4. Parametric study on improved strength

4.1. Analytical conditions

In the centrifuge model tests and their simulations, a case without ground improvement and two cases with different improvement strengths were conducted. In addition to the above three cases, which are the same as in the experiment, four different cases were added, as follows:

*Case assuming that the ground around the pile heads is improved by the sand compaction pile method ($q_u = 120$ kN/m^2)
*Case with an extremely highly stiff ground improvement, like concrete ($q_u = 40000$ kN/m^2)
*Two cases in which the stiffnesses of the improved ground were in between the above two cases.

Table 4 shows the cases of the parametric study. The stiffness of the improved ground in each case was calcu-

Table 4
Cases for parametric study on strength of improved ground.

No.	Unconfined compressive strength q_u [kN/m^2]	Young's modulus E [kN/m^2]	Note
1	120	8.50×10^4	Improved by sand compaction pile method
2	500	4.00×10^5	–
3	1100	8.82×10^5	Case-2 in experiment
4	3000	2.50×10^6	–
5	9030	7.53×10^6	Case-3 in experiment
6	40,000	3.10×10^7	Assuming concrete

lated from the relationship between the stiffness and the strength of concrete using the approximate formula for a concrete design (Japan Road Association, 2012b). For the input wave, in addition to the Level 1 earthquake shown in the road bridge specifications (Japan Road Association, 2012a), two waves were input for which the acceleration amplitude of the Level 1 earthquake was increased by 1.5 times and 2.0 times, respectively. At actual constructions, the specification design and construction management of the ground improvement are controlled by the compressive strength. In this study, however, the results are discussed in terms of the stiffness of the improved ground. This is because the improvement effect in the Level 1 earthquake, whereby the improved ground is not destroyed, is mainly examined.

4.2. Analytical results

Fig. 20 shows the time histories of the EPWPRs for the case without ground improvement. It can be confirmed that the larger the amplitude of the input wave is, the larger the increase in the EPWPR will be at any position. At GL − 1.5 m and GL − 2.75 m, the EPWPRs reach 1 in all patterns of input waves, and the ground liquefies. At GL. − 5.25 m and GL. −7.5 m in the non-liquefied layer, the EPWPRs do not reach 1 in any pattern and the magnitudes of the EPWPRs differ depending on the intensity of the input motion. As mentioned above, since the difference in
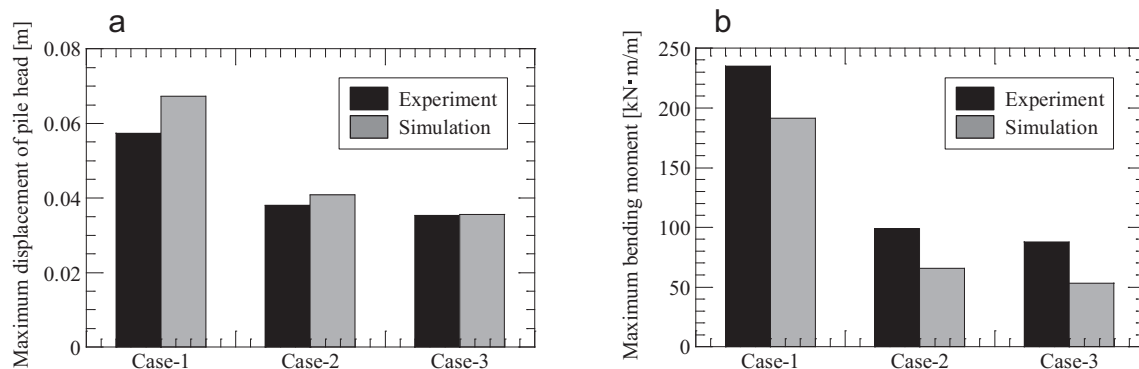

Fig. 19. Comparison of experimental and numerical results: (a) Maximum displacement of pile heads and (b) Maximum bending moments.
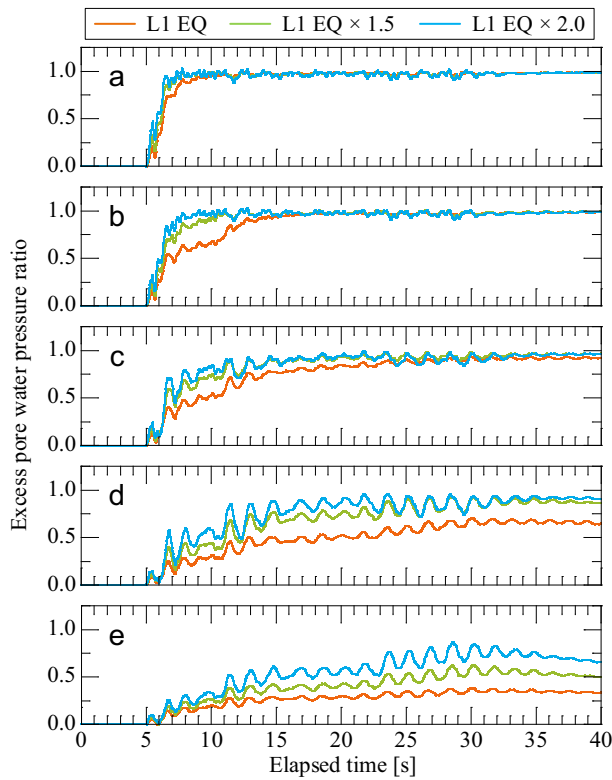
Fig. 20. Time histories of excess pore water pressure ratios of ground (parametric study): (a) GL −1.5 m, (b) GL −2.75 m, (c) GL −3.25 m, (d) GL −5.25 m, and (e) GL −7.5 m.

the EPWPRs affects the magnitude of the ground stiffness, it can be confirmed that the ground stiffness of the non-liquefied layer is significantly different due to the difference in the input seismic motion.

Fig. 21 shows the relationship between the stiffness of the improved ground and the maximum displacement of the pile heads (absolute value). When the Level 1 earthquake was input, the displacement of the pile heads became maximum at around 5.8 s for the cases in which the stiffness of the improved ground was $E = 2.50 \times 10^6$ kN/m^2 or more. The time when the displacement of the pile heads

becomes maximum changes depending on the stiffness of the ground improvement and the input seismic motion because the process of increasing the EPWPR differs in each case. Furthermore, it is considered that the vibration characteristics of the pile foundation might be changed by the different levels of stiffness of the improved ground. From Fig. 21, it can be confirmed that the higher the improved stiffness is, the greater the effect of reducing the displacement of the pile head will be, and the reduction rate converges to a constant value regardless of the magnitude of the input wave. Compared with the case of no ground improvement, the reduction rate of the Level 1 earthquake was 42%, Level 1 × 1.5 times was 58%, and Level 1 × 2 times was 66%. In other words, the larger the input seismic motion, the smaller the effect of reducing the displacement of the pile head by the ground improvement will be.

Fig. 22 shows the relationship between the stiffness of the improved ground and the maximum bending moment of the piles (absolute value). Similar to the displacement of the pile heads, the bending moments reached their maximum values at around 6 or 11 s. In the figure, the position where the maximum bending moment is generated can be seen. While the maximum bending moment is generated at the pile heads in the case without ground improvement, the maximum bending moment is generated at other parts of the piles in other cases. Furthermore, the maximum bending moment has been reduced by the improved ground. As the stiffness of the improved ground increased, although the displacement of the pile heads decreased, in terms of the bending moments, the position of the maximum bending moment changed, and there was optimum stiffness of the improved ground that minimized the maximum bending moment as a whole.

Fig. 23 shows the distribution of bending moments of the piles under the different levels of stiffness of the ground improvement. In the case with the smallest improved stiffness ($E = 8.5 \times 10^4$ kN/m^2), the position of the inflection point is around GL − 5.25 m. The bending moments at the pile heads and at the inflection point are reduced compared to the case without ground improvement. On the
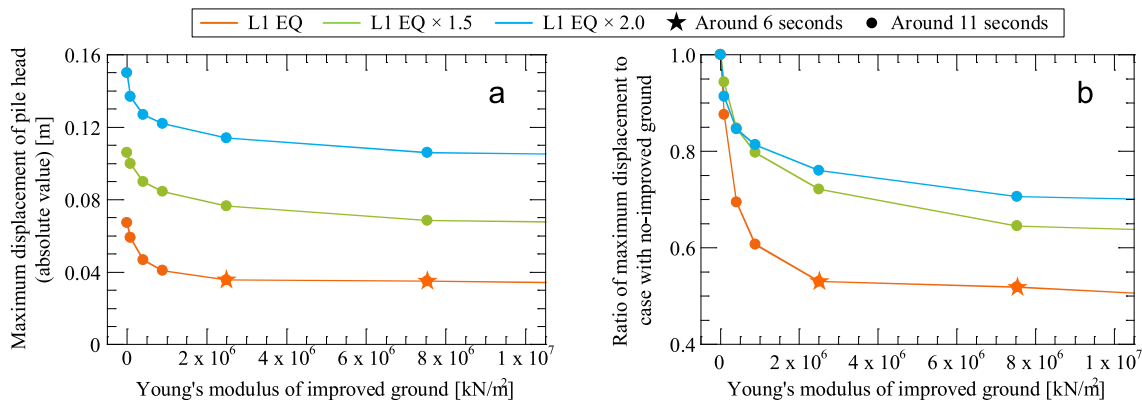

Fig. 21. Relationship between Young's modulus of improved ground and maximum displacement at pile heads: (a) Absolute value and (b) Ratio to case with no-improved ground.
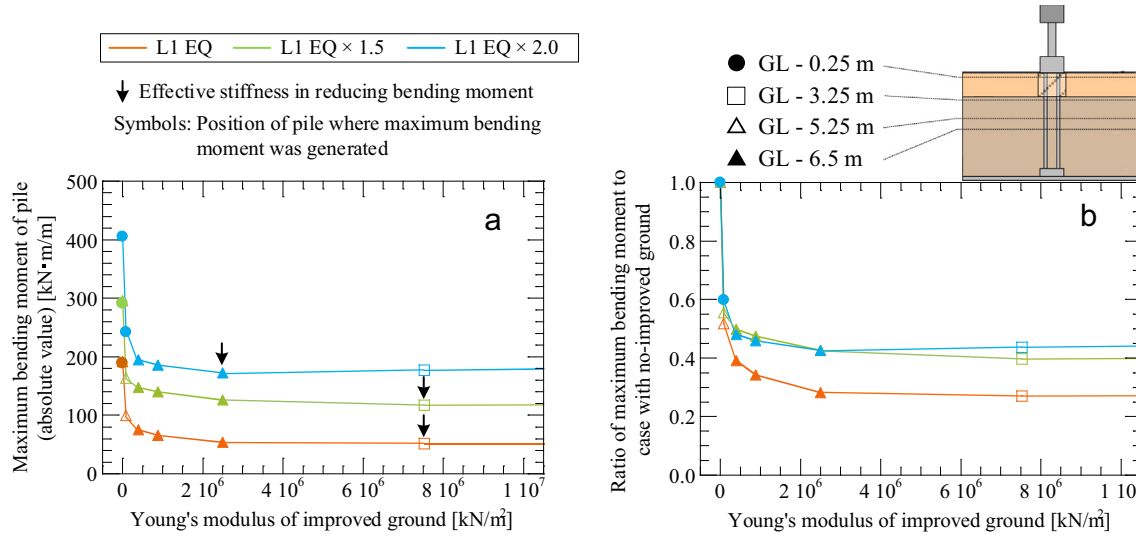
Fig. 22. Relationship between Young's modulus of improved ground and bending moments generated at pile: (a) Absolute value and (b) Ratio to case with no-improved ground.

other hand, when the stiffness of the improved ground is $E = 4.0 \times 10^5$ kN/m² or more, the bending moments at the pile heads becomes close to zero because the piles are restrained inside the improved ground, and the distribution is such that the footing is extended to the lower end of the improved ground (GL − 3.25 m). This tendency is similar to that when the coupling conditions of the pile heads are changed. Fig. 24 shows the similarity of the bending moment distribution of the pile foundation under different coupling conditions of pile heads and different levels of stiffness of the ground improvement around the pile heads.

As shown in Fig. 24a, the bending moment distribution of the piles differs depending on the coupling conditions of the pile heads. By making the pile heads flexible or with a semi-fixed connection, it is possible to allow the pile heads to rotate and distribute the bending moments generated at the pile heads and at the inflection point in the ground in a well-balanced manner. Similarly, as shown in Fig. 24b, the bending moment distribution for the piles with ground improvement is the same as when the foundation is extended to the lower end of the improved ground. This means that if the lower end of the improved ground is
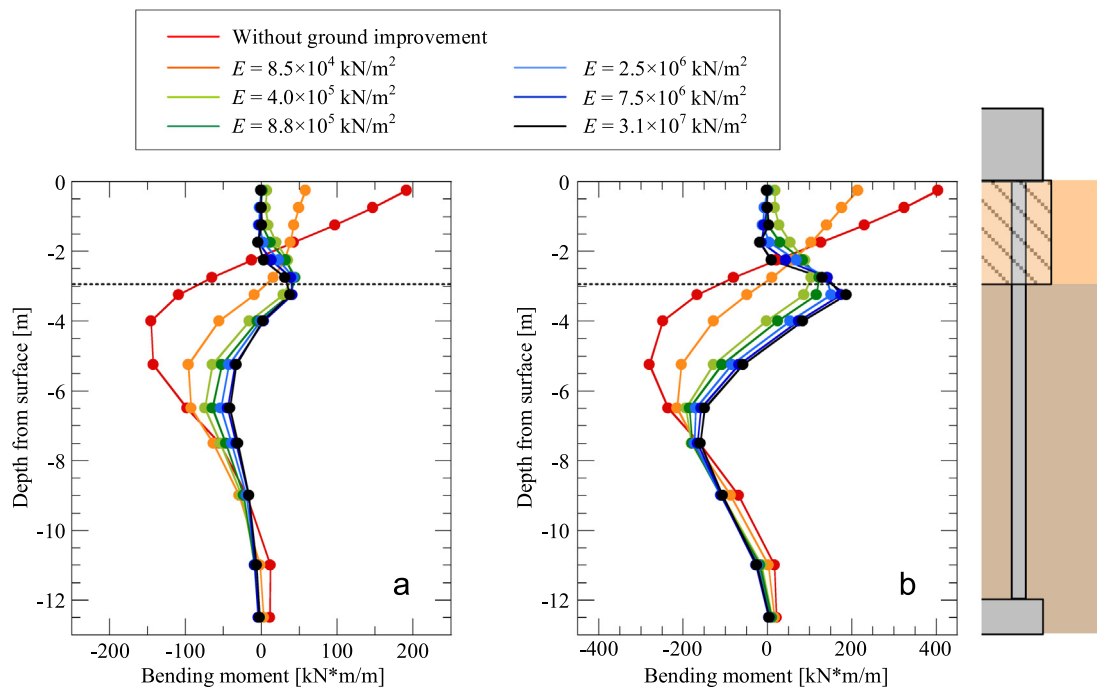

Fig. 23. Distribution of bending moments of pile under different levels of stiffness of ground improvement: (a) Level 1 earthquake and (b) Level 1 × 2.0 earthquake.
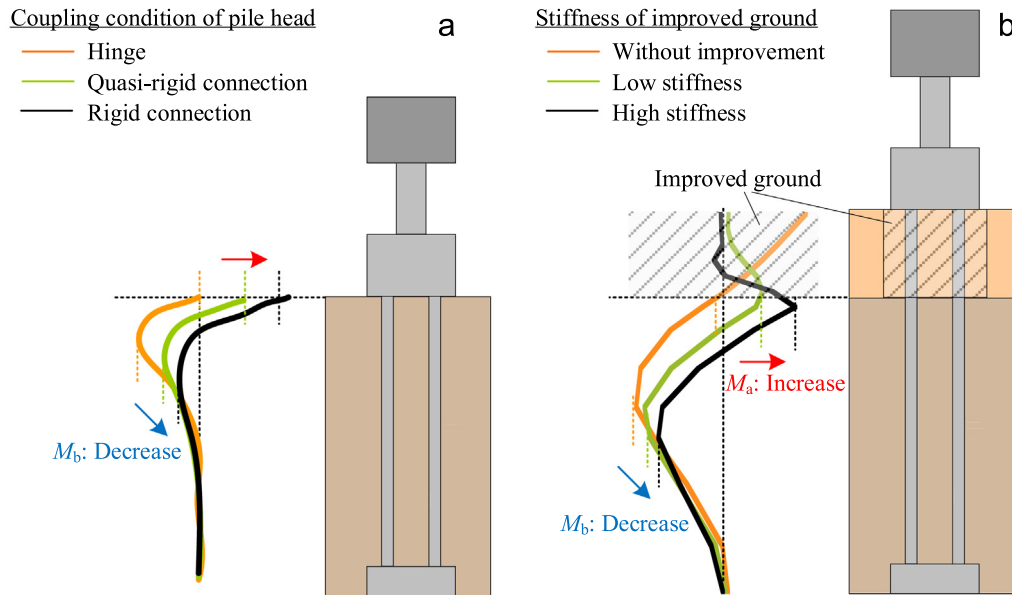
Fig. 24. Similarity of bending moment distribution of pile foundation under different coupling conditions of pile heads and different levels of stiffness of ground improvement around pile heads: (a) Coupling condition of pile heads and (b) Pile foundation with ground improvement.

regarded as a new pile head, increasing the stiffness of the improved ground will bring about the same results as increasing the degree of fixation of the pile head. In other words, it can be said that the structure is such that the footing is extended downward due to the ground improvement, and the behavior is like that of a combination of a caisson and piles.

5. Conclusions

In this study, centrifuge model tests and finite element analyses were conducted to clarify the effectiveness of applying a composite pile foundation with ground improvement to a liquefiable ground and to ascertain the improvement in strength (stiffness). The following conclusions have been obtained:

(1) It is possible to reduce the horizontal displacement of pile heads by improving the ground around the pile heads even in a liquefiable ground. By increasing the stiffness of the improved ground, a high reduction effect is exhibited. However, as the input seismic motion becomes larger, the reduction rate of the displacement decreases. This is because the amount of reduction of the displacement by the improved ground is smaller than the amount of increase in the response displacement due to the increase in input seismic motion.

(2) It is possible to reduce the bending moments of piles by improving the ground around the pile heads. However, the position where the maximum bending moment is generated changes depending on the stiffness of the improved ground, and there is an optimum value that minimizes the maximum bending moment as a whole. This is because the bending

moment at the inflection point in the non-liquefied layer cannot be sufficiently reduced when the stiffness of the improved ground is relatively low, while the bending moment at the lower part of the improved ground increases when the stiffness of the improved ground is high.

(3) The effect of the restraint of pile heads, brought about by the ground improvement, is similar to the effect when the degree of fixation of the pile heads is changed in a normal pile foundation. By improving the ground around the pile heads, the structure is such that the footing extends downward, and the behavior of the foundation is a combination of the behavior of a caisson and that of piles. Therefore, it is thought that the ground improvement alleviates extreme changes in the stiffness ratio at the boundary between the footing and the ground, and controls the bending moment distribution of the piles and the displacement of the pile heads.

References

Abdoun, T., Dobry, R., O'Rourke, T.D., Goh, S.H., 2003. Pile response to lateral spreads: Centrifuge modeling. J. Geotech. Geoenviron. Eng. 129 (10), 869–878. https://doi.org/10.1061/(ASCE)1090-0241(2003) 129:10(869).

Arulanandan, K., Sybico, J. 1992. Post-Liquefaction Settlement of Sand-Mechanism and in Situ Evaluation. In: Proc. of the 4th Japan-US Workshop on Earthquake Resistant Design of Lifeline Facilities and Countermeasures for Soil Liquefaction, Honolulu, HI, Technical Report NCEER 92-0019, pp. 239–247.

Asaoka, A., Nakano, M., Noda. T. 1998. Super loading yield surface concept for the saturated structured soils. In: Proc. of the 4th European Conference on Numerical Methods in Geotechnical Engineering-NUMGE98, pp. 232–242.

Asaoka, A., Noda, T., Yamada, E., Kaneda, K., Nakano, M., 2002. An elasto-plastic description of two distinct volume change mechanisms of soils. Soils Found. 42 (5), 47–57. https://doi.org/10.3208/sandf.42.5_47.

Bao, X., Morikawa, Y., Kondo, Y., Nakamura, K., Zhang, F., 2012. Shaking table test on reinforcement effect of partial ground improvement for group-pile foundation and its numerical simulation. Soils Found. 52 (6), 1043–1061. https://doi.org/10.1016/j.sandf.2012.11.020.

Bhattacharya, S., Madabhushi, S.P.G., Bolton, M.D., 2004. An alternative mechanism of pile failure in liquefiable deposits during earthquakes. Geotechnique 54 (3), 203–213. https://doi.org/10.1680/geot.54.3.203.36349.

Bhattacharya, S., Bolton, M.D., Madabhushi, S.P.G., 2005. A reconsideration of the safety of piled bridge foundations in liquefiable soils. Soils Found. 45 (4), 13–25. https://doi.org/10.3208/sandf.45.4_13.

Dewoolkar, M.M., Ko, H.Y., Stadler, A.T., Astaneh, S.M.F., 1999. A substitute pore fluid for seismic centrifuge modeling. Geotech. Test. J. 22 (3), 196–210. https://doi.org/10.1520/GTJ11111J.

Finn, W.D.L., Fujita, N., 2002. Piles in liquefiable soils: seismic analysis and design issues. Soil Dyn. Earthquake Eng. 22 (9–12), 731–742. https://doi.org/10.1016/S0267-7261(02)00094-5.

Hamada, M., O'Rourke, T.D., 1992. Case studies of liquefaction and lifeline performance during past earthquakes. Japanese case studies, vol. 1. Technical Rep. NCEER-92-0001. State University of New York, Buffalo, NY, pp. 1–28.

Hashiguchi, K., Ueno, M., 1977. Elastoplastic constitutive laws of granular material, Constitutive Equations of Soils. In: Murayama, S., Schofield, A.N. (Eds.), Proc. of the 9th International Conference on Soil Mechanics and Foundation Engineering, pp. 73–82.

Japan Road Association, 2012. Specifications for highway bridges Part V: Seismic Design.

Japan Road Association, 2012. Specifications for highway bridges Part III: Concrete Bridges.

Kheradi, H., Morikawa, Y., Ye, G., Zhang, F., 2019. Liquefaction-Induced Buckling Failure of Group-Pile Foundation and Countermeasure by Partial Ground Improvement. Int. J. Geomech. 19 (5), 04019020. https://doi.org/10.1061/(asce)gm.1943-5622.0001379.

Maeda, Y., Omine, K., Ochiai, H., Furuki, H., Naemura, S., Okochi, Y., Ichikawa, A., 2006. Improvement of horizontal bearing capacity by composite ground foundation method in soft ground. In: Proc. of the 22th US-Japan Bridge Engineering Workshop, Seattle, WA, USA.

Maeda, Y., Omine, K., Ochiai, H., Furuki, H., Naemura, S., Okochi, Y., 2007. Design and Evaluation of a New Composite Foundation of Pile with DMM to Control the Lateral Deformation during Earthquake. In: Kyriazis, D.P. (Eds.), Proc. of the 4th International Conference on Earthquake Geotechnical Engineering, Thessaloniki, Greece, Paper No. 1189.

Okamura, M., Inoue, T., 2012. Preparation of fully saturated models for liquefaction study. Int. J. Phys. Model. Geotech. 12 (1), 39–46. https://doi.org/10.1680/ijpmg.2012.12.1.39.

Phanikanth, V.S., Choudhury, D., Reddy, G.R., 2013. Behavior of single pile in liquefied deposits during earthquakes. Int. J. Geomech. 13 (4), 454–462. https://doi.org/10.1061/(ASCE)GM.1943-5622.0000224.

Rollins, K.M., Adsero, M.E., Herbst, M.A., Lemme, N., 2010. Ground Improvement for Increasing Lateral Pile Group Resistance. In: Proc. of 5th International Conference on Recent Advances in Geotechnical Earthquake Engineering and Soil Dynamics, San Diego, CA, Paper No. OSP 9.

Rollins, K.M., Gerber, T.M., Lane, D., Ashford, S.A., 2005. Lateral Resistance of a Full-Scale Pile Group in Liquefied Sand. J. Geotech. Geoenviron. Eng. 131 (11), 115–125. https://doi.org/10.1061/(ASCE)1090-0241(2005)131:1(115).

Shinohara, M., Moro, T., Yamagishi, T., 2015. Partial Strengthening of Pile Foundation using Soil Improvement for Liquefaction in Sanbo Junction. Bridge Found. Eng. 49 (6), 29–34 (in Japanese).

Stewart, D.P., Chen, Y.R., Kutter, B.L., 1998. Experience with the use of methylcellulose as a viscous pore fluid in centrifuge models. Geotech. Test. J. 21 (4), 365–369. https://doi.org/10.1520/GTJ11376J.

Tamura, K., Azuma, T., Kobayashi, H., Morimitsu, T., Sato, N., 1999. Experimental Study on Reduction of Horizontal Subgrade Reaction due to Liquefaction, Technical Report of PWRI, No. 3697 (in Japanese).

Tomisawa, K., Kimura, M., 2017. New Technology on Seismic Reinforcement of Pile Foundation for Long Life Bridges. Procedia Eng. 171, 1035–1042. https://doi.org/10.1016/j.proeng.2017.01.443.

Tomisawa, K., Miura, S., 2007. Mechanical behavior of pile foundation constructed in composite ground and its evaluation. Soils Found. 47 (5), 961–972. https://doi.org/10.3208/sandf.47.961.

Tomisawa, K., Nishimoto, S., Miura, S., 2008. Earthquake resistance of pile foundations in composite ground through dynamic nonlinear numerical analysis. In: Proc. of 14th World Conference on Earthquake Engineering, Beijing, China.

Wilson, D.W., Boulanger, R.W., Kutter, B.L., 2000. Observed seismic lateral resistance of liquefying sand. J. Geotech. Geoenviron. Eng. 126 (10), 898–906. https://doi.org/10.1061/(ASCE)1090-0241(2000)126:10(898).

Ye, B., Ye, G.L., Zhang, F., Yashima, A., 2007. Experiment and numerical simulation of repeated liquefaction-consolidation of sand. Soils Found. 47 (3), 547–558. https://doi.org/10.3208/sandf.47.547.

Yoshida, N., Finn, W.D.L., 2000. Simulation of liquefaction beneath an impermeable surface layer. Soil Dyn. Earthquake Eng. 19 (5), 333–338. https://doi.org/10.1016/S0267-7261(00)00018-X.

Zhang, F., Jin, Y., Ye, B., 2010. A try to give a unified description of Toyoura sand. Soils Found. 50 (3), 679–693. https://doi.org/10.3208/sandf.50.679.

Zhang, F., Kimura, M., Nakai, T., Hoshikawa, T., 2000. Mechanical behavior of pile foundations subjected to cyclic lateral loading up to the ultimate state. Soils Found. 40 (5), 1–17. https://doi.org/10.3208/sandf.40.5_1.

Zhang, F., Ye, B., Noda, T., Nakano, M., Nakai, K., 2007. Explanation of cyclic mobility of soils: Approach by stress-induced anisotropy. Soils Found. 47 (4), 635–648. https://doi.org/10.3208/sandf.47.635.

Zhang, F., Ye, B., Ye, G.L., 2011. Unified description of sand behavior. Front. Archit. Civ. Eng. China 5 (2), 121–150. https://doi.org/10.1007/s11709-011-0104-z.